Influence of Microstructure on the Thermal Fatigue Behavior of a Cast Cobalt-Base Superalloy

M. FRANÇOIS and L. RÉMY

The influence of microstructure on the thermal fatigue (TF) behavior of MAR-M 509, a cast cobalt-base superalloy, was investigated using a burner rig and wedge-type specimens which were submitted to thermal shock from 200 °C to 1100 °C. Two microstructures were studied: a coarse microstructure using specimens machined from bulk castings and a fine microstructure using cast-to-size specimens. Metallographic observations showed that cast-to-size specimens display a gradient in microstructure since the size of secondary dendrites increases with the distance to the thin edge. As high-temperature fatigue in this superalloy is controlled by oxidation-fatigue interactions, the kinetics of interdendritic oxidation was studied at 900 °C. Interdendritic oxidation was found to be inhibited by a refinement of dendritic microstructure. A fine microstructure was shown to give a much longer TF life-to-crack initiation and a much lower crack growth rate. This behavior was mainly related to differences in interdendritic oxidation since interdendritic areas act as crack initiation sites as well as easy crack propagation paths. The influence of microstructure on crack growth rates was accounted for by using a previously proposed oxidation-fatigue crack growth model and interdendritic oxidation kinetic data.

I. INTRODUCTION

THERMAL fatigue (TF) is one of the primary life-limiting factors of machinery components due to startup and shutdown operations, especially for turbine blades and inlet guide vanes in jet engines. Tests of actual components in servicelike conditions are very expensive, and thermal cycling of blade or vane edges is usually simulated by tests of simple structures. Glenny and coworkers in the late 1950's introduced a fluidized bed technique using tapered disc specimens.[1,2,3] Other authors later used wedge-type specimens and fluidized beds[4] or a burner rig.[5] For a long time, these tests were mainly used to compare the TF resistance of candidate materials for turbine components. Spera later showed that such tests can be used to assess TF life predictions[6,7] using a damage model and computation of stress-strain loops at the periphery of the disc or the thin edge of wedge-type specimens.

Blades and vanes in jet engines have been made for a number of years from conventionally cast superalloys.[8,9] The TF resistance of such alloys is usually evaluated using cast-to-size tapered discs or wedge specimens. Thus, the periphery of the disc or the thin edge of the wedge specimen have a fine microstructure (*i.e.*, fine grain size and small primary and secondary dendrite arm spacings) which is often assumed to be fairly representative of actual components.[9]

Basic mechanical properties, on the other hand, and especially low-cycle fatigue (LCF) data or creep-rupture curves are established on test specimens which are most often machined from bulk castings. Most data used in design procedures come from specimens which can have a much coarser microstructure than cast-to-size TF specimens due to large differences in solidification conditions. Laboratory specimens made from conventionally cast alloys seldom have the same microstructure as actual components.

A detailed study of the TF behavior of MAR-M* 509, a cast cobalt superalloy, was completed recently in our laboratory.[10,11] This alloy is used in inlet guide vanes. Damage under TF cycling[10,11] as well as under LCF cycling at high temperature[12,13] has been shown to involve oxidation fatigue interactions in this alloy. The oxidation of interdendritic areas which bear out primary MC carbides has been shown to play a major role in fatigue damage of this alloy,[12] and its kinetics was previously reported for a coarse microstructure.[16] A fatigue crack growth model has been proposed for this alloy with a coarse microstructure to describe oxidation-fatigue interactions,[14,15] and it was shown to account for LCF life at high temperature for various test conditions[13] and crack growth curves under TF cycling.[10] Care was taken in this previous study to machine TF wedge-type specimens and LCF specimens from bulk castings. Thus, TF and LCF specimens have the same coarse microstructure, which is coarser than that in cast-to-size components or TF specimens.

The influence of casting microstructure on the TF behavior of MAR-M 509 was therefore studied. A single-wedge specimen geometry, as defined in previous work,[10] was used with specimens either cast-to-size or machined from bulk castings. This paper first reports the variation in microstructure in the cast-to-size specimens and its influence on the kinetics of interdendritic oxidation. Then TF test results on cast-to-size and machined specimens are described. Results are discussed then, and in particular, the fatigue crack growth model mentioned earlier[14,15] is used with oxidation kinetic data to rationalize the influence of microstructure on the TF crack growth behavior.

*MAR-M is a trademark of Martin Marietta Industries.

M. FRANÇOIS, formerly with the Centre des Matériaux, Ecole des Mines de Paris, is with Heurchrome, Saint-Ouen L'Aumone, France. L. RÉMY is with the Centre des Matériaux, Ecole des Mines de Paris, URA CNRS 866, BP 87, 91003 Evry Cedex, France.

Manuscript submitted July 12, 1989.

II. MATERIAL AND EXPERIMENTAL PROCEDURE

A. *Material*

The composition of the master heat used in this study was, in weight percent, 0.59C-11Ni-23.2Cr-6.95W-3.31Ta-0.30Zr-0.22Ti-0.17Fe-0.008B-0.005P-0.003S-balance Co. Thermal fatigue specimens with a coarse microstructure were machined from bulk castings. Cast-to-size specimens were made using precision investment casting to have a fine microstructure. All of the specimens were heat-treated for 6 hours at 1230 °C.

The coarse microstructure has been described in some detail in earlier publications.[10,12] The average grain size is 0.8 mm, which corresponds approximately to the size of primary dendrites. The alloy is mainly a cobalt-base solid solution which contains small MC carbides about 1 μm in size which precipitate during the treatment at 1230 °C.[12] Eutectic interdendritic phases precipitate during casting, *i.e.*, lamellar chromium-rich $M_{23}C_6$ carbides, which then degenerate during the heat treatment (volume fraction about 1.5 pct), and tantalum-rich MC carbides, which have a Chinese-script morphology (volume fraction about 2.4 pct). The mean secondary dendrite size defined as the mean intercept between interdendritic areas is about 100 μm (this mean intercept is used here for convenience instead of secondary dendrite arm spacing, about 60 μm, to make measurements easier in the cast-to-size microstructure).

The cast-to-size specimens exhibit a fine microstructure which has a size gradient from the thin edge to the bulk part of the specimen. As interdendritic oxidation is the primary factor in high-temperature fatigue damage, only the mean secondary dendrite size was measured to characterize the fine microstructure. Mean intercept values will be described in Section III–A.

B. *Thermal Fatigue Specimens*

Wedge specimens 55-mm long were used. Their cross section is shown in Figure 1 (specimen type A in Reference 10) with an edge radius of 0.25 mm. Machined TF specimens with a coarse microstructure were heat-treated at 1100 °C for 1 hour and air cooled after machining to remove surface strains at the thin edge due to machining. Microhardness recovers its usual value using this procedure (Vickers microhardness under a 0.98 N load decreases from about 500 after machining to about 400 after postmachining heat treatment). The same heat treatment was applied to cast-to-size TF specimens. All of the TF specimens were then mechanically polished lengthwise down to 3-μm diamond paste in a manner similar to LCF specimens.

C. *Thermal Fatigue Tests*

Tests were carried out on the TF rig of Société Nationale d'Etude et de Construction de Moteurs d'Aviation (SNECMA), Corbeil, France. The TF specimen is simply placed on three vertical silica rods. The thin edge is in a horizontal plane and is alternately exposed to cooling and heating nozzles. The specimen is uniformly heated along its thin edge by the flame of a burner using a mixture of air and propane gas for 60 seconds and then it is cooled down by compressed air for 20 seconds. The vertical displacement of the cooling and heating nozzles is *via* a pneumatic actuator. The pressure inside the test chamber is lowered *via* an exhaust fan.

An instrumented specimen with welded thermocouples near the thin edge was used to adjust testing conditions: air and propane flow for heating; compressed air flow for cooling. Details of instrumentation were given elsewhere.[10] The same maximum temperature was maintained for every test sequence using this dummy test piece. This specimen was removed and replaced by the test specimen without any welded thermocouple. A thermocouple protected by an alumina tube was put in simple contact with the specimen surface to check the reproducibility of testing conditions throughout the sequence.

The specimens were exposed to a thermal cycle that ranged from 1100 °C to 200 °C at the thin edge. Tests were periodically interrupted to inspect the specimen surfaces. The length of most cracks was monitored using a binocular optical microscope at magnifications of 30 and 75 times. This method was used only for cracks longer than 0.1 to 0.2 mm. Shorter cracks were observed in a scanning electron microscope. Only the evolution of the major crack, which generally formed first, is reported here. The specimen was turned upside down after each test interruption so that eventual asymmetry effects caused by cooling and heating could be minimized. The crack depth is reported here using a calibration procedure from surface measurements as previously discussed.[10]

Observations were made of the specimen surface as well as the lengthwise sections of tested specimens using optical and scanning electron microscopy (SEM).

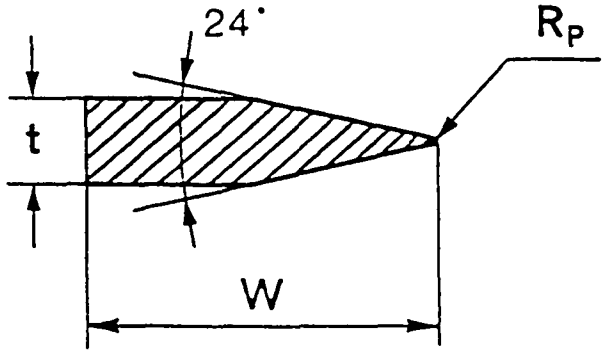

TYPE	W (mm)	R_p (mm)	t (mm)
A	27.60	0.25	6.7
LENGTH			55 (mm)

Fig. 1—Cross section of the TF wedge specimen.

D. *Measurements of Interdendritic Oxidation Kinetics*

Static oxidation was studied on cast-to-size TF specimens which were sectioned perpendicularly to the thin edge. Specimen surface preparation was kept identical to that of cycled specimens. Specimens were exposed to air in a furnace at 900 °C; this temperature was chosen since it gives rise to a fairly strong oxidation in the coarse microstructure. Exposure times of 20 and 96 hours were mainly used, and some measurements were also made after 5 hours.

Observations were carried out on the cross sections of oxidized specimens using a scanning electron microscope. A nickel layer was deposited on the oxidized specimens before observation, and specimens were handled carefully to minimize oxide spalling. Measurements were mainly concerned with interdendritic oxide spikes which grow inwardly into the metal. The depth of oxidized carbides was defined as including the whole matrix thickness with about 20 to 30 measurements in each area studied, as previously done by Reuchet and Rémy for MAR-M 509 with a coarse microstructure.[16]

III. RESULTS

A. *Microstructure and Oxidation Kinetics in the Cast-to-Size Specimens*

Figure 2 shows typical areas of an oxidized specimen which were exposed to air at 900 °C for 20 hours at various distances from the thin edge. A large variation in microstructure is evident in the micrographs. In the immediate vicinity of the thin edge, secondary dendrites are very small. Their mean intercept is about 5 μm. When the distance to the thin edge increases, the microstructure becomes coarser, and the dendrite size increases.

In the coarse microstructure, interdendritic MC carbides showed a typical Chinese-script morphology (Figure 3).[16] In the vicinity of the thin edge of cast-to-size specimens, they look globular on a specimen section; however, deep etching showed that these MC carbides are, in fact, interconnected rods.[17] The proportion of Chinese-script MC carbides increases with increasing distance from the thin edge.

The average dendrite size was measured as a function of the distance (x) to the thin edge. Results are shown in Figure 4. The average dendrite size increased from about 5 μm at the thin edge to 40 μm at 5 mm from the edge. Thus, there is a very large size gradient of the microstructure in the cast-to-size specimen: it varies from very fine in the immediate vicinity of the thin edge to much coarser farther from the edge.

As evidenced by Figure 2, this variation in dendrite microstructure gives rise to variations in oxidation morphology. The thickness of the oxide scale is rather small at the thin edge, with very short oxide spikes growing along interdendritic areas. At 1 mm from the edge, the oxide scale is thicker, and interdendritic oxidation goes deeper in the alloy. This trend is confirmed at larger distances from the edge.

Oxidation along interdendritic carbides has been studied for the coarse microstructure by Reuchet and Rémy.[16]

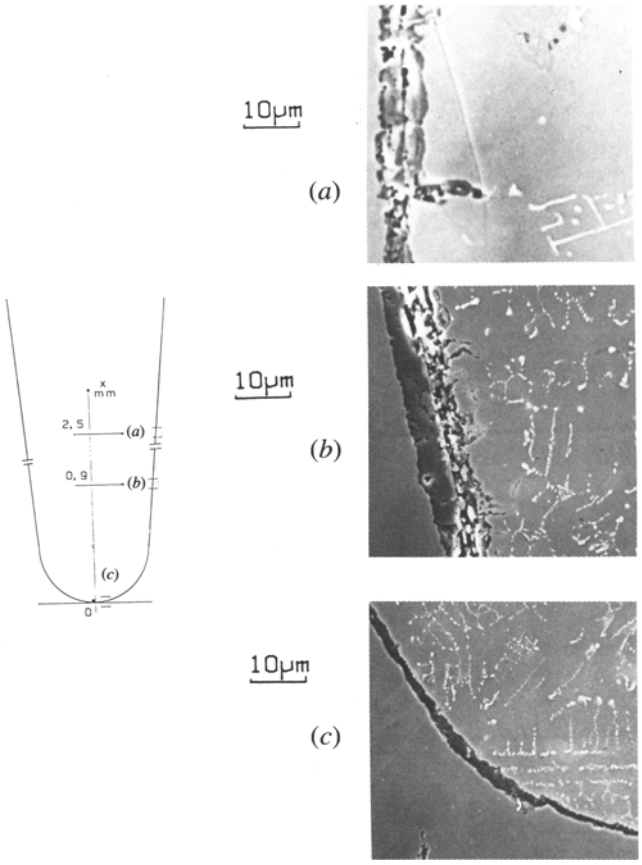

Fig. 2—Metallographic section of a cast-to-size wedge specimen which has been oxidized in a furnace at 900 °C for 20 h; micrographs [(*a*) 2.5 mm from the edge, (*b*) 0.9 mm from the edge, and (*c*) at the edge] show the large variation in oxide scale and microstructure with distance from the thin edge.

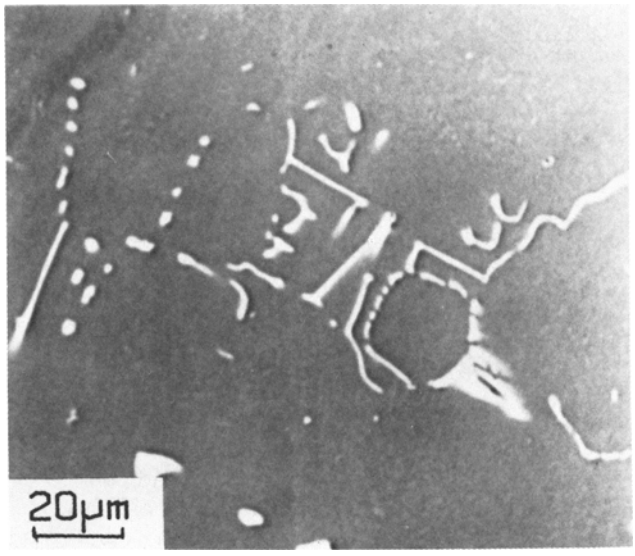

Fig. 3—Typical Chinese-script morphology in the wedge specimens with a coarse microstructure (the scale of the carbide microstructure is to be compared with Fig. 2).

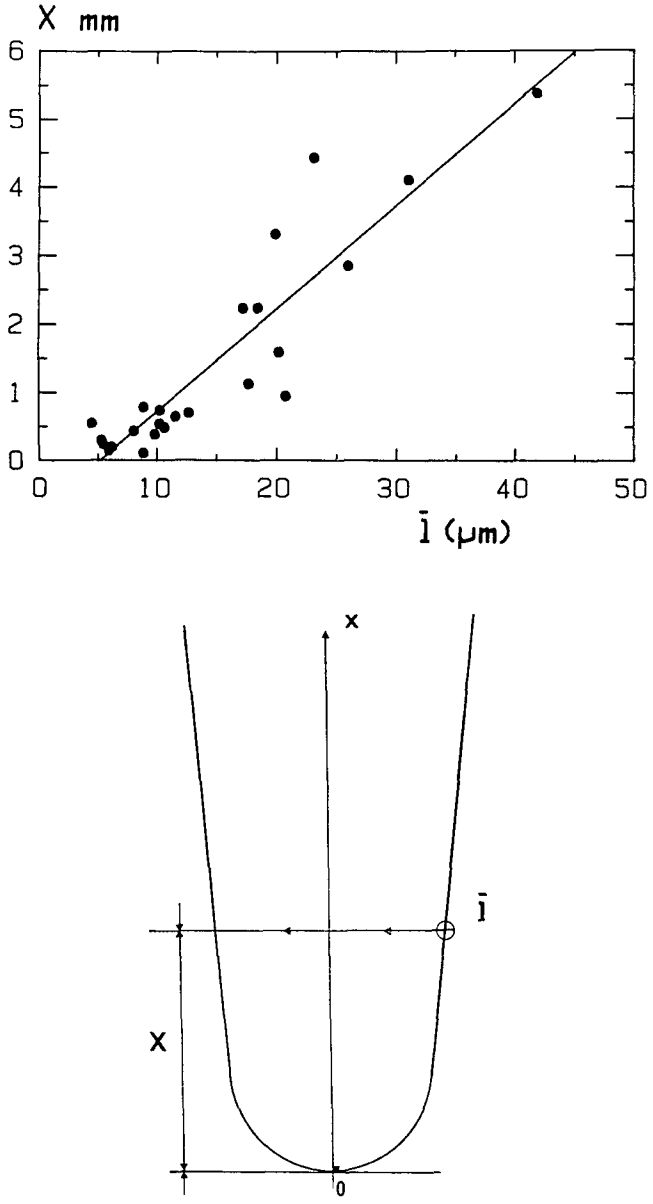

Fig. 4—Variation of the average secondary dendrite size ($\bar{l}$) as a function of the distance from the thin edge (x) in the cast-to-size wedge specimen.

The penetration of oxide was measured along the direction of the interdendritic area from the external oxide scale. They found that the average interdendritic oxide depth, l_{ox}, obeys the following kinetics:

$$l_{ox} = \alpha_c t^{1/4} \qquad [1]$$

when the thickness of the matrix oxide scale varies as $t^{1/2}$, as usually reported for overall oxidation. The usual parabolic kinetics for matrix oxide is in agreement with the solution of Fick's equation in a semi-infinite plane. The boundary conditions for that diffusion equation are completely different for interdendritic oxidation and could be related to classical solutions of grain boundary diffusion. The simple model of Fischer[18] actually predicts a $t^{1/4}$ kinetics for grain boundary diffusion which gives theoretical support to the present experimental observations. The gradient in oxygen concentration was measured using an electron microprobe and was found to be consistent with theoretical expectations.[19]

The average depth of interdendritic oxide spikes, l_{ox}, is plotted *vs* exposure time in log-log coordinates in Figure 5 for two areas in the cast-to-size specimens: the area within 0.8 mm from the thin edge and the area about 2.5 mm from the thin edge. These measurements are in good agreement with a $t^{1/4}$ kinetics, but the oxidation kinetics is slower for the cast-to-size specimen than for the coarse microstructure previously studied. Furthermore, the interdendritic oxidized depth for a given exposure time is shorter for material at the thin edge than at some distance from it. The interdendritic oxidation kinetics is thus definitely slower when the secondary dendrites are smaller in size.

The secondary dendrite size was measured in the same area as the depth of oxide spikes in order to get a more precise relationship between secondary dendrite size and oxidation kinetics. The oxidation constant, α_c, was deduced from the average oxide depth in a given area and from the exposure time (5, 20, or 96 hours) at 900 °C using Eq. [1]. This value of α_c is plotted *vs* the size of secondary dendrites in Figure 6. In spite of experimental scatter, there is a linear increase of the oxidation constant, α_c, with dendrite size up to 20 μm: a fourfold increase of dendrite size from 5 to 20 μm yields a fourfold increase of α_c. The variation of α_c tends to vanish when the microstructure becomes coarser. The oxidation constant for the coarse microstructure (average secondary dendrite size about 100 μm) is almost the same as in the cast-to-size specimen at 5 mm from the thin edge (average dendrite size about 40 μm).

The inhibition of interdendritic oxidation at small dendrite sizes can be easily understood. A small secondary dendrite size is accompanied by an increase in the density of interdendritic areas per unit volume. Therefore, the amount of microsegregation will be decreased, especially chromium and tantalum, which precipitate as interdendritic carbides during the late stages of solidification.[12,20] This will favor smaller carbide sizes, as

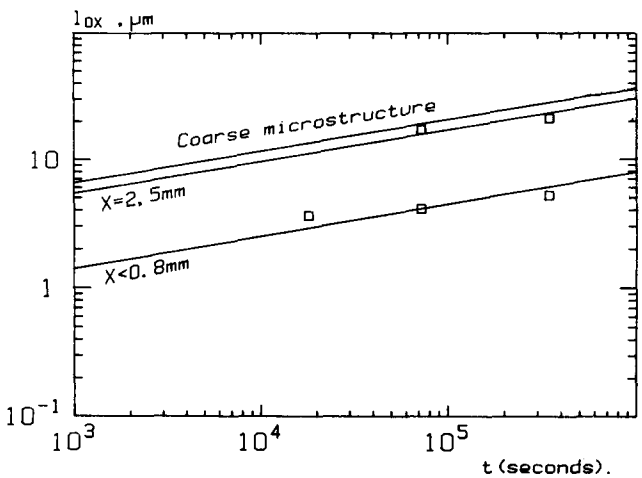

Fig. 5—Variation of the average oxide spike depth (l_{ox}) with exposure time at 900 °C (t) in log-log coordinates; curves are plotted for the area within 0.8 mm of the thin edge and at 2.5 mm from the thin edge in the cast-to-size and compared with the curve for the coarse microstructure.

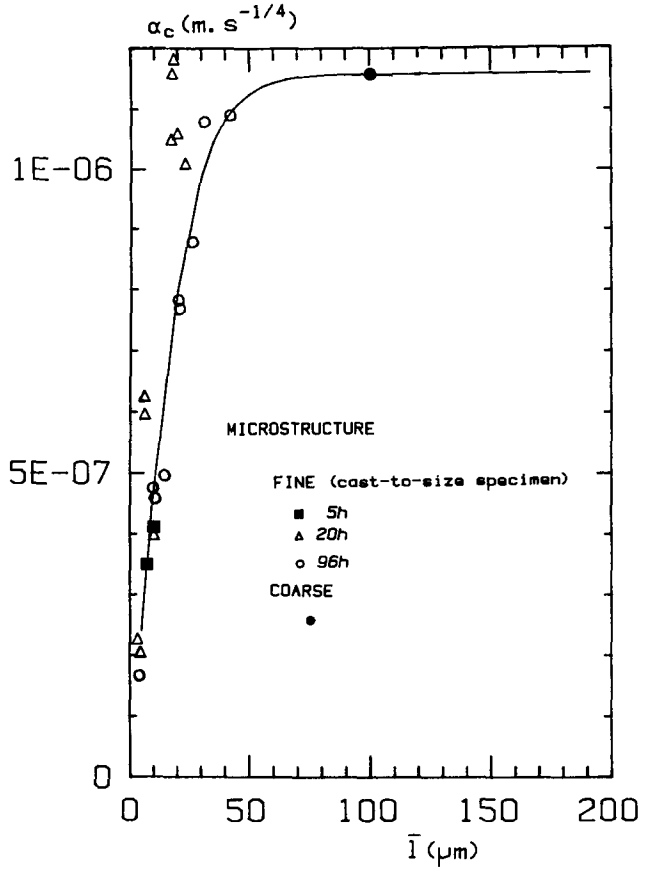

Fig. 6—Variation of the interdendritic oxidation constant (α_c) with the average secondary dendrite size ($\bar{l}$).

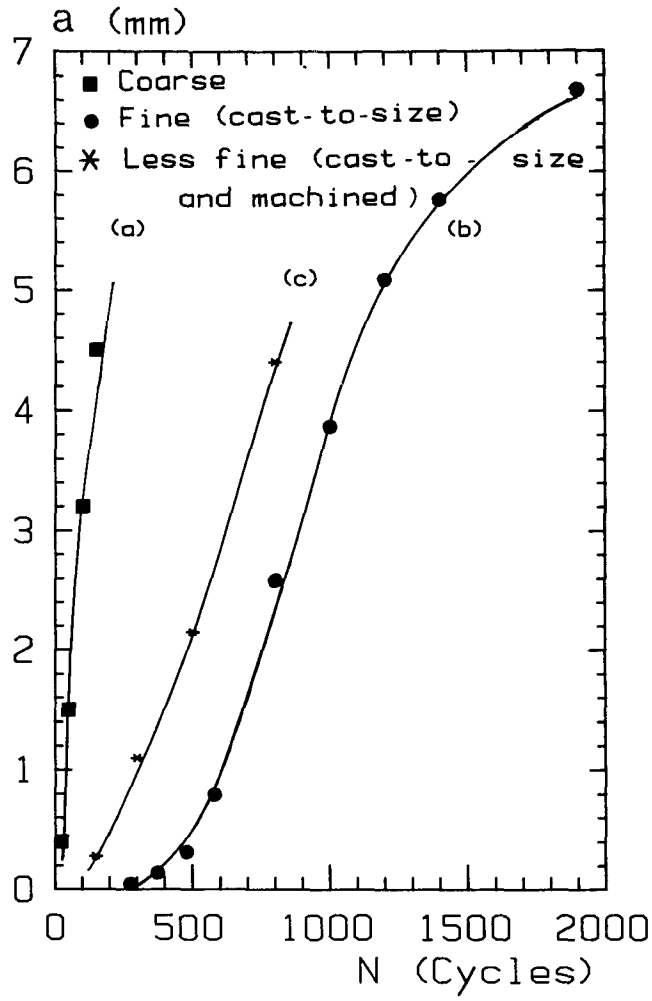

Fig. 7—Variation of the major crack depth as a function of the number of thermal fatigue cycles; curves labeled (a), (b), and (c) refer to a specimen with a coarse microstructure, a cast-to-size specimen with a fine microstructure, and a cast-to-size and machined specimen with a less fine microstructure, respectively.

detailed solidification studies on nickel-base alloys have demonstrated.[21] The carbide density per unit area in interdendritic areas will be lower and will inhibit the kinetics of interdendritic oxidation. The larger number of diffusion paths for inward diffusion of oxygen (due to the larger density of interdendritic areas intersecting the free surface) will also inhibit the inward growth of oxide spikes.

B. *Thermal Fatigue Experiments*

The variation in depth of the major crack is plotted as a function of the number of cycles in Figure 7 for the coarse microstructure (referred to as (a)) and for the cast-to-size specimen with a fine microstructure (referred to as (b)). The curve for the coarse microstructure refers to the average of two different specimens when a single specimen was used for the fine microstructure.

Cracks nucleate very early in TF specimens with a coarse microstructure. Cracks initiate at preferentially oxidized Chinese-script MC carbides[10] and can be observed after 10 TF cycles (Figure 8). The life-to-crack initiation, N_i, can be defined, for instance, when the depth of the major crack reaches 0.3 mm. This life-to-crack initiation is very small, about 20 cycles for the coarse microstructure, but is more than 20 times longer for the cast-to-size specimen.

The crack growth rate is very high in the specimens with a coarse microstructure, *i.e.*, about 50 μm/cycle, and nearly constant up to a depth of a few millimeters. Then the crack slows down. The evolution of crack depth with the number of cycles is rather different for the cast-to-size specimen. First, the crack growth rate is very low, about 40 times smaller than for the coarse microstructure at the thin edge. Then the crack growth rate increases

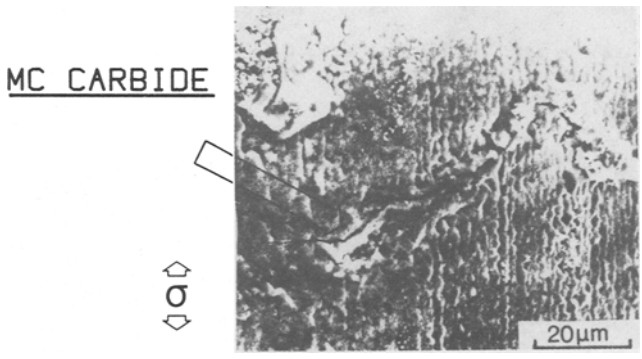

Fig. 8—Crack initiation at a preferentially oxidized MC carbide in a specimen with a coarse microstructure after 10 thermal cycles.

with crack depth and becomes constant when the crack is deeper than about 0.8 mm. This constant crack growth rate regime occurs up to 4-mm crack depth; then crack growth slows down.

Metallographic observations of TF specimens were reported previously for the coarse microstructure.[10] The crack path is mainly along interdendritic MC carbides and shows a substantial amount of interdendritic oxidation (Figure 9). Figure 10 shows that the same features are observed in the finer microstructure of the cast-to-size specimen.

Specimens sectioned at the thin edge after TF test completion show extensive interdendritic oxidation in coarse and fine microstructures (Figure 11). The external surface was roughened by TF cycling, and interdendritic areas look as if they were extruded from the bulk alloy. This surface aspect could be caused by spallation of matrix oxide between interdendritic areas[22] since the thickness of matrix oxide is much less than expected from isothermal oxidation kinetics.[23]

The tremendous influence of specimen processing on life-to-crack initiation and on crack growth rate in the vicinity of the thin edge should be the consequence of the large differences in casting microstructures. Moreover, the continuous increase in crack growth rate of the cast-to-size specimen should reflect the increase in dendrite size which was observed. A complementary experiment was made to further document this hypothesis. A thin layer of material 0.25 mm in thickness was removed by machining each side of the wedge of a cast-to-size specimen. A new thin edge was then machined in this specimen, which gives rise to a small reduction in specimen width but mainly produces a less fine microstructure in the thin edge: the secondary dendrite size increases from about 6 to 13 μm.

The evolution of the major crack depth is plotted in Figure 7 as a function of the number of cycles. The crack growth curve almost parallels that of the original cast-to-size specimen but with two major differences. First, the life-to-crack initiation has been given a threefold reduction. Then the crack growth rate is almost constant from the thin edge up to 4 mm. This result bears out the hypothesis that the large crack growth rate variation up to 0.8 mm in the cast-to-size specimen mainly arose from a size gradient of microstructure in the vicinity of the thin edge.

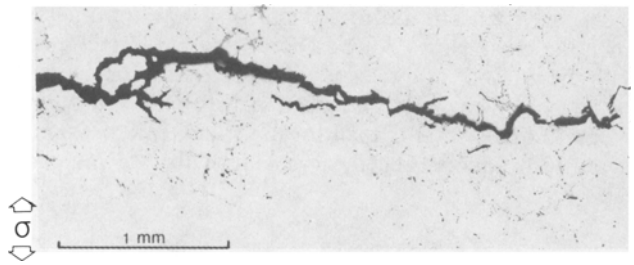

Fig. 9—Crack propagation path in a TF specimen with a coarse microstructure (optical microscopy).

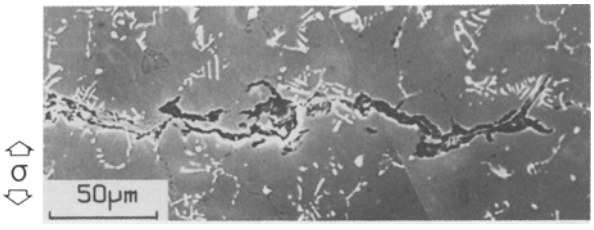

Fig. 10—Crack propagation path in a cast-to-size TF specimen (SEM).

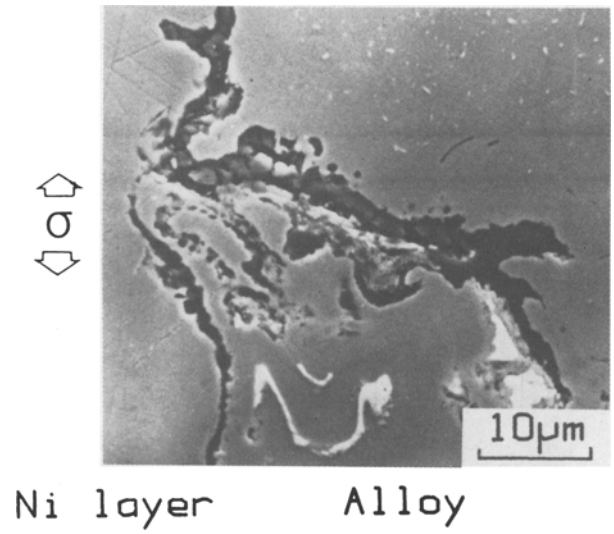

(*a*)

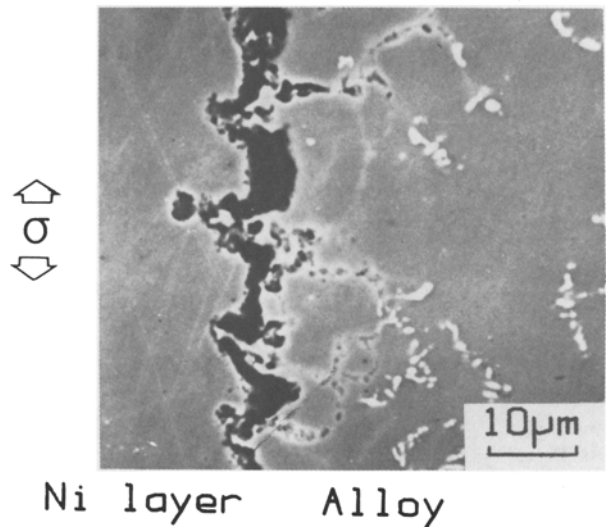

(*b*)

Fig. 11—Oxides on longitudinal sections of TF specimens at the thin edge (*a*) with a coarse microstructure and (*b*) with a fine microstructure (cast-to-size specimen).

IV. DISCUSSION

This study has compared the resistance to TF cracking of specimens of MAR-M 509 superalloy with either a coarse or fine microstructure using specimens which were machined from bulk castings or cast-to-size, respectively. The influence of microstructure was clearly evidenced for the experimental conditions investigated.

The influence of secondary dendrite size on the number of cycles needed to initiate a major crack 0.3-mm deep and on the crack growth rate in the vicinity of the thin edge is summarized in Figures 12 and 13, respectively. The life-to-crack initiation is shown to decrease rapidly with increasing secondary dendrite $\bar{l}$ (it varies approximately as the inverse of dendrite size). Crack initiation in high-temperature fatigue of cast nickel alloys was associated with cracking of the external oxide scale at regions of high stress concentrations, particularly interdendritic areas.[22] A finer microstructure gives rise to a better resistance to interdendritic oxidation, as shown in this study, and should reduce the stress concentrations induced by volume changes when MC carbides transform to oxides.[12] Such an effect could superimpose with a conventional grain-type refinement effect which is known to improve resistance to fatigue crack initiation.[24] Comparison with the literature is difficult since the influence of casting microstructure on TF life-to-crack initiation (and crack growth) is poorly documented. Woodford and Mowbray[9] mainly considered the influence of grain size in cast superalloys and showed that a finer grain size improves the life-to-crack initiation. They pointed out, however, that TF cracks were mainly interdendritic and that the influence of microstructure was much more complex than simply a grain size effect. Beck and Santhanam[25] claimed that a larger secondary dendrite size improves life-to-crack initiation in MAR-M 509. They investigated only a small range of dendrite arm spacings (35 to 60 μm), however, in which interdendritic oxidation kinetics is almost insensitive to dendrite size according to the present work.

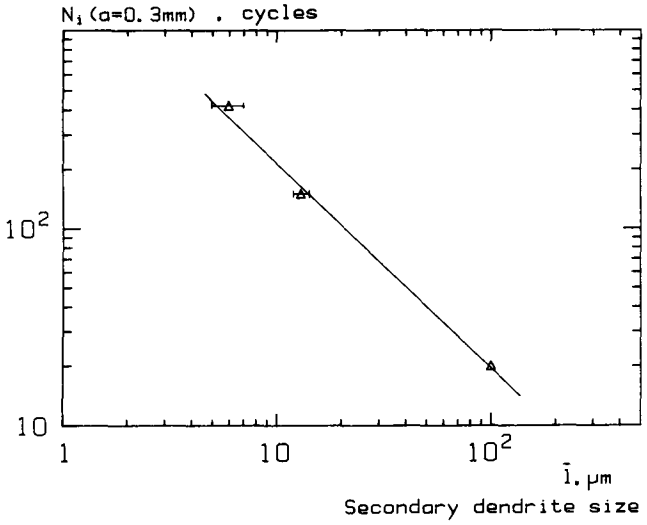

Fig. 12—Variation of the TF life-to-crack initiation, N_i, (defined to 0.3-mm crack depth) as a function of the secondary dendrite size at the thin edge.

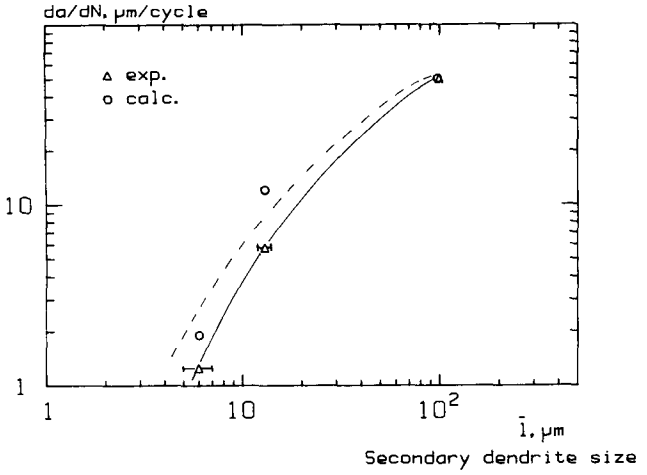

Fig. 13—Variation of the TF crack growth rate in the vicinity of the thin edge (da/dN) as a function of secondary dendrite size. Experimental data as well as calculated values as described in the text are shown.

The crack growth rate in the vicinity of the thin edge increases drastically with increasing secondary dendrite size (Figure 13) (here, again, an opposite trend was claimed to be observed by Beck and Santhanam[25]). This effect is believed not to reflect an effect of dendrite size *per se* but to be induced by the variation of interdendritic oxidation kinetics which has been observed to occur with dendrite size (Figure 6). Fatigue crack growth rate (FCGR) would be expected to be only weakly dependent of dendrite size in the absence of oxidation, as it has been shown for the grain size dependence of FCGR of short cracks; a finer grain size even gives rise to a larger growth rate in the case of long cracks,[26] *i.e.*, the trend opposite to that of the present results. Here, a coarser dendrite size induces more segregated interdendritic areas, which, in turn, triggers interdendritic oxidation kinetics. This could thus explain why a coarse dendrite microstructure has a much higher TF crack growth rate, which would not be expected in the absence of oxidation. However, the microstructure dependence of crack growth rate can be discussed in a quantitative manner using a model recently proposed by Rezai-Aria and Rémy[14,15] and computations of the stress-strain-temperature history of TF wedge specimens.

These computations were recently completed for MAR-M 509 with a coarse microstructure.[11] The analysis method used a finite element computation of the temperature field and a uniaxial calculation of the stress-strain cycle in every point of the specimen using a cyclic viscoplastic constitutive equation (since the strain tensor has one major principal strain). The influence of maximum temperature and of specimen geometry was reported in detail elsewhere.[10]

A fatigue crack growth model has been proposed which takes into account the interaction between oxidation and fatigue. All model parameters besides oxidation constants were deduced from experiments on compact tension (CT) specimens. These latter were isothermal experiments on either virgin material or on precracked CT specimens, which were then oxidized at high temperature. In particular, experiments on preoxidized CT specimens showed much higher crack growth rates than on virgin material. A material zone of the previous crack tip had thus been altered by oxidation, and electron microprobe analysis has shown oxygen diffusion ahead of the crack tip to be responsible for this behavior. A diffusion model was used to relate the oxygen concentration gradient to the depth of interdendritic oxide.

These experiments on CT specimens were analyzed using a "local approach," *i.e.*, using the local stresses

at the crack tip which are deduced from finite element computation.[14,15] As a uniaxial stress analysis is used for TF specimens, only the uniaxial form of these equations is recalled here.

For a cycle under varying temperature, the elementary damage increment is defined over a characteristic distance, λ, ahead of the crack tip, which is taken as the secondary dendrite size ($\lambda = 100\ \mu m$ for the coarse microstructure), as

$$dD/dN = (\Delta\sigma/2S_0)^M/\{(1 - R)(\sigma_c^* - \sigma)/S_0\}^\beta \quad [2]$$

with $R = \langle 1 - \Delta\sigma/\sigma \rangle$. (The symbol $\langle U \rangle = U$ if $U \geq 0$ and $\langle U \rangle = 0$ if $U < 0$.) In Eq. [2], S_0, M, and β are three constants at a given temperature and

$$\sigma_c^* = \text{Min}\{\sigma_f, \sigma_c(t, T)\} \quad [3]$$

where σ_f is the monotonic fracture stress of virgin material and σ_c is that of the material ahead of the crack tip which is embrittled by oxygen diffusion in front of the oxide. Finally,

$$\sigma_c(t, T) = \sigma_{co}[1 - u + u \exp(m\lambda/l_{ox})] \quad [4]$$

where u is temperature-dependent and m is a constant. The term l_{ox} is the depth of interdendritic oxide and is given by

$$d(l_{ox})/dt = \int_0^{\Delta t} \alpha_c^4(t) \times dt/\Delta t \quad [5]$$

where Δt is the cycle period and α_c is the oxidation constant, as in Eq. [1], and is defined from isothermal oxidation kinetic measurements. The number of cycles to get a crack growth increment of size λ is given by the following condition:

$$\int_0^{N(\lambda)} dD = 1 \quad [6]$$

The crack growth rate is deduced as

$$da/dN = \lambda/N(\lambda) \quad [7]$$

Equation [2] has to be used at an equivalent temperature under nonisothermal loading. This temperature is not uniquely defined and can be either the temperature of the maximum stress or that of the minimum stress. The parameter $N(\lambda)$ was taken as the geometric mean of the values computed in each case.

This model has been used for MAR-M 509 with a coarse microstructure and was shown to account for frequency and wave shape effects in high-temperature fatigue as well as for maximum temperature and specimen geometry effects in TF.[14,15]

This model was thus used to analyze the results of the present study using two main assumptions: first, the stress-strain behavior of MAR-M 509 was supposed to be, in a first approximation, insensitive to secondary dendrite size as well as the crack growth rate in the absence of oxidation. Therefore, all of the parameters of the model, with the exception of oxidation constants, were assumed to remain unaltered. Second, the influence of microstructure on oxidation kinetics was supposed to be independent of temperature. So, if $\alpha_c(T, \bar{l})$ is the interdendritic oxidation constant at a given temperature, T, and for a secondary dendrite size, $\bar{l}$, it can be deduced from the value for the coarse microstructure, $\alpha_c(T, \bar{l}_c)$, as

$$\alpha_c(T, \bar{l}) = \alpha_c(T, \bar{l}_c) \times \alpha_c(900\ ^\circ\text{C}, \bar{l})/\alpha_c(900\ ^\circ\text{C}, \bar{l}_c) \quad [8]$$

The oxidation constant was computed at any point of the specimen using the variation of the oxidation constant, α_c, at 900 °C defined as a function of secondary dendrite size, $\bar{l}$, as

$$\alpha_c(900\ ^\circ\text{C}, \bar{l}) = \alpha_\infty \tanh^{-1}(\bar{l}/\bar{l}_\infty)$$

where α_∞ and $\bar{l}_\infty$ are two constants, and the dendrite size was supposed to vary linearly with distance to the thin edge (fitted curve is shown as a solid line in Figure 6).

The crack growth rate, da/dN, in the vicinity of the thin edge was computed along these lines for the coarse microstructure, the cast-to-size specimen (fine microstructure), and the cast-to-size and machined specimen (less fine microstructure) and is within a factor of 2 of the experimental values, as shown in Figure 13. Furthermore, computed crack growth curves (crack depth *vs* the number of cycles spent in crack propagation) are in good agreement with experimental curves for the coarse microstructure and the cast-to-size specimen (Figures 14 and 15). A constant crack growth rate is predicted over

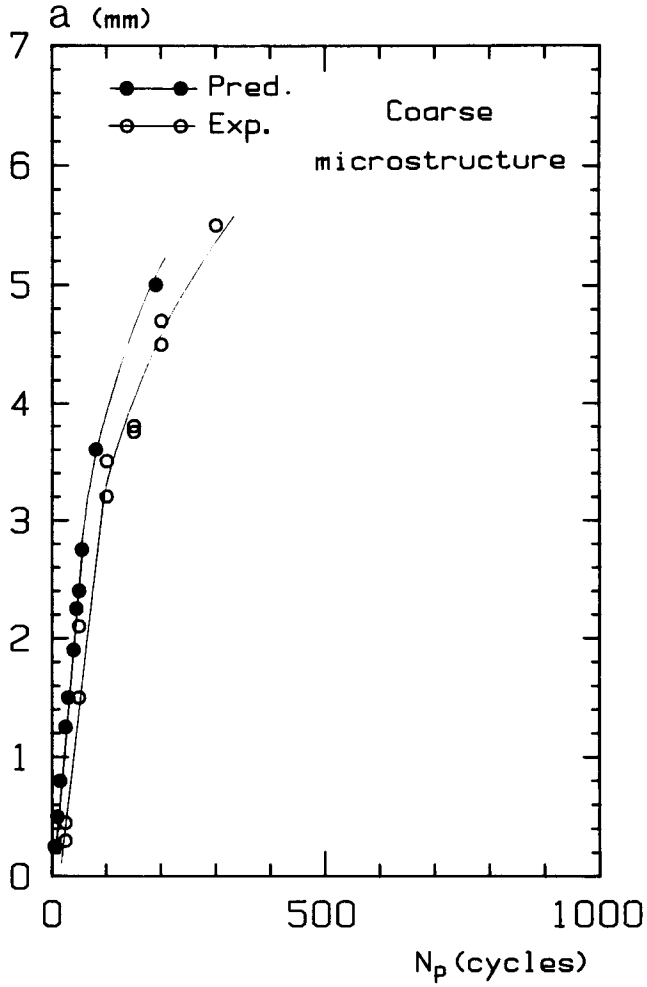

Fig. 14—Comparison between experimental and predicted variations of crack depth (a) *vs* the number of TF cycles spent in crack propagation (N_p) for the coarse microstructure.

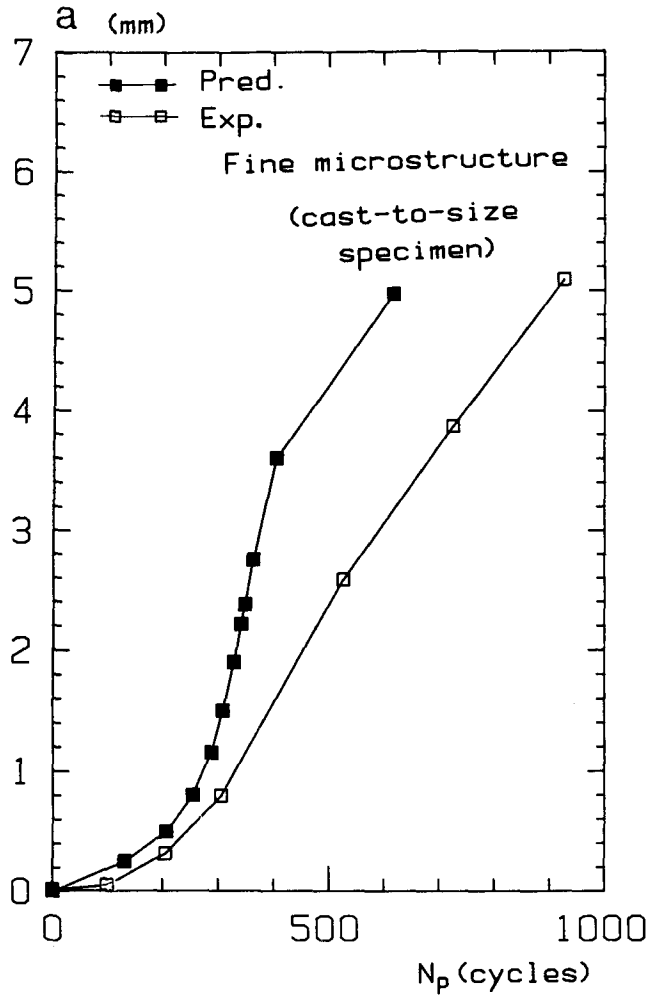

Fig. 15—Comparison between experimental and predicted variations of crack depth (a) *vs* the number of TF cycles spent in crack propagation (N_p) for the cast-to-size specimen with a fine microstructure.

a large range of crack depth for the coarse microstructure, as actually observed. A constant crack growth rate regime is only predicted for cracks deeper than 1 mm in the cast-to-size specimen. The strong increase of crack growth rate for cracks growing from the thin edge up to 1 mm is actually accounted for. This increase in growth rate results from the increase in secondary dendrite size with distance from the thin edge (from 5 to 14 μm), which, in turn, gives rise to a linear increase of the interdendritic oxidation constant, α_c. The model for oxidation fatigue crack growth can account for the major features of TF crack growth. The influence of secondary dendrite size on TF crack growth rate is mostly due to its effect on interdendritic oxidation kinetics. This model shows, in agreement with experiment, that a small dendrite size can drastically reduce TF crack propagation rate, but only when it is smaller than about 20 μm. The influence of dendrite size is weaker at larger sizes since the oxidation constant becomes less sensitive to microstructure.

This study has shown that high-temperature fatigue data, as obtained from laboratory tests using specimens machined from bulk castings, with a coarse microstructure, are not directly transferable to component design. The actual microstructure of cast components has to be accounted for, but depending upon alloy chemistry and casting conditions, the discrepancy between the lifetime for a coarse microstructure and that for the actual microstructure can be large or not. Modeling interactions between oxidation and fatigue seems to be a promising way to handle the microstructure dependence of lifetime under thermal-mechanical cycling.

V. CONCLUSIONS

This study of the influence of casting microstructure on the TF behavior has shown that the TF resistance of MAR-M 509 superalloy is controlled by the size of secondary dendrites.

A fine dendritic size tremendously improves the number of cycles to initiate a crack as well as the resistance to crack growth under TF cycling. This influence of secondary dendrite size is, to a large extent, the consequence of its effect on the kinetics of interdendritic oxidation.

Cast-to-size wedge specimens actually possess a large gradient in microstructure, since machining the thin edge decreases both the resistance to crack initiation and to crack growth.

The microstructure dependence of TF crack growth rate has been rationalized using a previously proposed oxidation fatigue crack growth model and the kinetics of interdendritic oxidation. This model has shown that the influence of secondary dendrite size on the crack growth rate under TF can be accounted for solely by its effect on interdendritic oxidation kinetics.

ACKNOWLEDGMENTS

The authors are indebted to SNECMA for provision of tested material. Messrs. Y. Honnorat, J.P. Aubert, and F. Millet from the Materials and Processes Department of SNECMA have kindly provided access to their TF testing facilities, and their collaboration is gratefully acknowledged.

REFERENCES

1. E. Glenny, J.E. Northwood, S.W.K. Shaw, and T.A. Taylor: *J. Inst. Met.*, 1958–59, vol. 87, pp. 294-302.
2. E. Glenny and T.A. Taylor: *J. Inst. Met.*, 1959–60, vol. 88, pp. 449-61.
3. E. Glenny: in *Thermal and High Strain Fatigue*, Institute of Metals, Iron Steel Institute, London, 1967, pp. 346-63.
4. P.T. Bizon and D.A. Spera: in *Thermal Fatigue of Materials and Components*, ASTM STP 612, D.A. Spera and D.F. Mowbray, eds., ASTM, Philadelphia, PA, 1976, pp. 106-22.
5. F. Rezai-Aria, L. Rémy, C. Herman, and B. Dambrine: *Mechanical Behaviour of Solids IV*, J. Carlson and M.G. Ohlson, eds., Pergamon Press, Oxford, 1983, vol. 1, pp. 247-53.
6. D.A. Spera: *Calculations of Thermal Fatigue Life Based on Accumulated Creep Damage*, NASA TND-5589, National Aeronautics and Space Administration, Washington, DC, 1969.
7. D.A. Spera: in *Fatigue at Elevated Temperatures*, ASTM STP 520, ASTM, Philadelphia, PA, 1972, pp. 648-57.
8. C.T. Sims and W.C. Hagel: *The Superalloys*, Wiley, New York, NY, 1972, p. 14, p. 403.
9. D.A. Woodford and D.F. Mowbray: *Mater. Sci. Eng.*, 1974, vol. 16, pp. 5-43.
10. F. Rezai-Aria, M. François, and L. Rémy: *Fatigue Fract. Eng. Mater. Struct.*, 1988, vol. 11, pp. 277-89.

11. F. Rezai-Aria, B. Dambrine, and L. Rémy: *Fatigue Fract. Eng. Mater. Struct.*, 1988, vol. 11, pp. 291-302.
12. J. Reuchet and L. Rémy: *Mater. Sci. Eng.*, 1983, vol. 58, pp. 19-32 and 33-42.
13. L. Rémy, F. Rezai-Aria, R. Danzer, and W. Hoffelner: in *Low Cycle Fatigue*, ASTM STP 942, H.D. Solomon, G.R. Halford, L.R. Kaisand, and B.N. Leis, eds., ASTM, Philadelphia, PA, 1988, pp. 1115-32.
14. F. Rezai-Aria and L. Rémy: *Proc. Int. Spring Meeting*, Fatigue Committee of the Société Francaise de Métallurgie, Paris, June 9–11, 1986, pp. 290-301.
15. F. Rezai-Aria and L. Rémy: *Eng. Fract. Mech.*, 1989, vol. 34, pp. 283-94.
16. J. Reuchet and L. Rémy: *Metall. Trans. A*, 1983, vol. 14A, pp. 141-49.
17. J. Reuchet and L. Rémy: Centre des Matériaux, Ecole des Mines de Paris, unpublished research, 1980.
18. J.C. Fischer: *J. Appl. Phys.*, 1951, vol. 22, p. 74.
19. L. Rémy, M. François, and M. Reger: Centre des Matériaux, Ecole des Mines de Paris, unpublished research, 1983.
20. J.M. Drapier, V. Leroy, C. Dupont, D. Coutsouradis, and L. Habraken: *Cobalt*, 1968, vol. 41, pp. 199-213.
21. R. Fernandez, J.C. Lecomte, and T.Z. Kattamis: *Metall. Trans. A*, 1978, vol. 9A, pp. 1381-86.
22. M. Reger and L. Rémy: *Metall. Trans. A*, 1988, vol. 19A, pp. 2259-68.
23. M. François: *Rôle de l'oxydation dans l'endommagement en fatigue thermique de l'alliage MAR-M 509*, Mémoire CNAM, Paris, 1989.
24. J.C. Grosskreutz: *Phys. Status Solidi B*, 1971, vol. 47, pp. 11-31.
25. C.G. Beck and A.T. Santhanam: in *Thermal Fatigue of Materials and Components*, ASTM STP 612, D.A. Spera and D.F. Mowbray, eds., ASTM, Philadelphia, PA, 1976, pp. 123-40.
26. C.W. Brown, J.E. King, and M.A. Hicks: *Met. Sci.*, 1984, vol. 18, pp. 374-80.